# Donor-Acceptor Pairs in Wide-Bandgap Semiconductors for Quantum Technology Applications

Anil Bilgin,<sup>1,\*</sup> Ian N. Hammock,<sup>1</sup> Jeremy Estes,<sup>1</sup> Yu Jin,<sup>2</sup> Hannes Bernien,<sup>1</sup> Alexander A. High,<sup>1,3</sup> and Giulia Galli<sup>1,2,3,†</sup>

<sup>1</sup>Pritzker School of Molecular Engineering, University of Chicago, Chicago, Illinois 60637, USA

<sup>2</sup>Department of Chemistry, University of Chicago, Chicago, IL 60637, USA

<sup>3</sup>Center for Molecular Engineering and Materials Science Division,

Argonne National Laboratory, Lemont, Illinois 60439, USA

(Dated: May 11, 2023)

We propose a quantum science platform utilizing the dipole-dipole coupling between donor-acceptor pairs (DAPs) in wide bandgap semiconductors to realize optically controllable, long-range interactions between defects in the solid state. We carry out calculations based on density functional theory (DFT) to investigate the electronic structure and interactions of DAPs formed by various substitutional point-defects in diamond and silicon carbide (SiC). We determine the most stable charge states and evaluate zero phonon lines using constrained DFT and compare our results with those of simple donor-acceptor pair (DAP) models. We show that polarization differences between ground and excited states lead to unusually large electric dipole moments for several DAPs in diamond and SiC. We predict radiative lifetimes and photoluminescence spectra for selected substitutional atoms and show that while B-N pairs in diamond are challenging to control due to their large electron-phonon coupling, DAPs in SiC, especially Al-N pairs, are suitable candidates to realize long-range optically controllable interactions.

#### I. INTRODUCTION

The search for a quantum architecture that can be easily fabricated, addressed, and manipulated has been at the forefront of academic, industrial, and defense efforts [1]. Realizing such an architecture will enable us to engineer new quantum technologies. Diamond and silicon carbide (SiC) have been demonstrated to be suitable platforms to engineer devices for quantum teleportation [2], quantum networks [3], and quantum memories [4, 5]. The promise of such a solid state systems is driven by the possibility of harnessing spin-spin interactions between color centers and their surrounding nuclear spins, and additionally by establishing entangled photonic links [3, 4, 6]. However, current implementations of solid-state qubits are limited to the length scale (several angstroms) of spin-spin interactions, or to macroscopic distances of meters to kilometers associated with quantum networks [4, 7]. Both of these implementations have several drawbacks. The former relies upon stochastic formation of color centers and nuclear sites, and at present, nanofabrication techniques cannot engineer devices on the angstrom scale [8]. On the other hand, large scale network platforms require entanglement protocols based on probabilistic photon detections that often occur on time-scales much longer than the qubit's coherence time [9, 10]. These shortcomings may be overcome with the introduction of a system possessing coherent, long-range (> 10 nm) interactions, and addressable optical transitions. Long-range interactions within the solid-state are

particularly interesting as they would enable desirable on-chip entanglement schemes and protocols to improve state-of-the-art methods [11–13].

Many promising avenues have been explored over the years in search of interactions stronger than spin-spin interactions. For instance, in cuprous oxide, manipulation of giant Rydberg excitons with principal quantum numbers of up to n=25 has been demonstrated [14]. The strong, long-range dipole-dipole interactions from these excitons could be used to create solid-state analogues of Rydberg atoms [15]. Unfortunately, it has been difficult to produce high crystal quality artificial cuprous oxide and the observation of such higher excited states is made possible by the comparatively large Rydberg energy of around 100 meV [14]. The specific conditions required for the realization of this class of systems might hamper their generalization to other host materials. Another interesting class of systems are donor-acceptor pairs (DAPs) in semiconductors. The transition between ionized donors and acceptors has been theoretically modeled and experimentally observed in many materials, including silicon [16, 17], silicon carbide [18–20], diamond [21, 22], and other compound semiconductors [23–26]. Even though donor-acceptor pair (DAP) systems have been extensively studied for decades, only recently they have been considered for applications in quantum information science. For instance, efficient DAP emission in hexagonal boron nitride has recently been proposed as an alternative way of generating single photon sources for quantum technologies [27]. Assembling DAPs with well-defined donor-acceptor distances and orientations in covalently-linked organic molecules might also prove to be a promising approach for manipulation and coherent control of spin states [28, 29]. However, compared to molecular systems, DAPs in the solid-state have the

<sup>\*</sup> bilgin@uchicago.edu

<sup>†</sup> gagalli@uchicago.edu

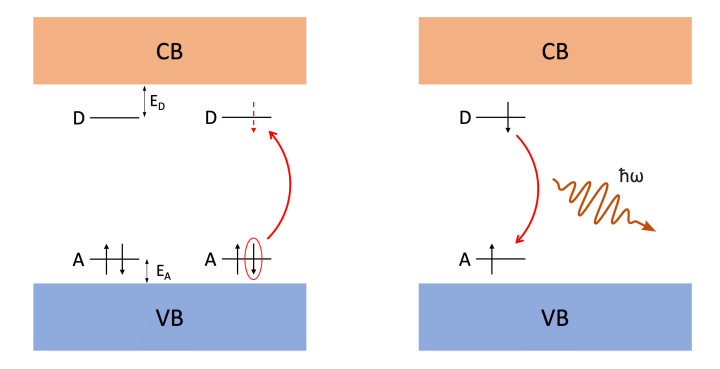


**FIG. 1:** Electronic structure of a donor (D) acceptor (A) pair in the ground (left) and excited (right) states.  $E_D$  and  $E_A$  are the donor and acceptor binding energies and VB and CB denote valence band and conduction band of the host material, respectively. A photon is emitted as a result of the recombination of a hole bound to the acceptor and an electron bound to the donor.

advantage of making use of mature nanofabrication and control techniques for implementation on a chip in a scalable manner.

One crucial property of DAPs that could allow the realization of emergent quantum phenomena in solids is their static electric dipole moments that can be optically controlled, similar to Rydberg atoms in vacuum. This dipole is due to the donor and the acceptor remaining charged after the electron and hole pair recombine to produce a photon. A brief description of the electronic ground and excited states of DAPs is given in Figure 1. The strength of this dipole depends on the distance between the donor and the acceptor, and it can be engineered by placing the impurities at specific distances in the host lattice, as illustrated in Figure 2.

Here, we propose a new quantum science platform utilizing the static electric dipole-dipole coupling between DAPs in wide bandgap semiconductors to realize optically controllable, long-range interactions in the solid-state. The host crystal could then be interfaced with nano-control devices using nanofabrication techniques. In our proposed platform, pair-pair interactions are mediated by the optically switchable dipole-dipole coupling similar to Rydberg interactions in atomic systems [30, 31]. This coherent interaction is governed by Coulomb's law, and depends on the pair-pair distance and orientation. Hence it can extend over a significantly longer length scale (> 10 nm) than spin-spin interactions. With new developments in growth and synthesis techniques [8], it might be possible to create arrays of DAPs with well-defined pair distances and orientations, similar to molecular systems. Additionally, DAPs in solid-state systems have the advantage of easily-fabricated control infrastructures such as cavities and waveguides. Moreover, DAP lifetimes of up to tens of microseconds [17], or even up to milliseconds [32] have already been observed. These lifetimes are much longer than the hun-

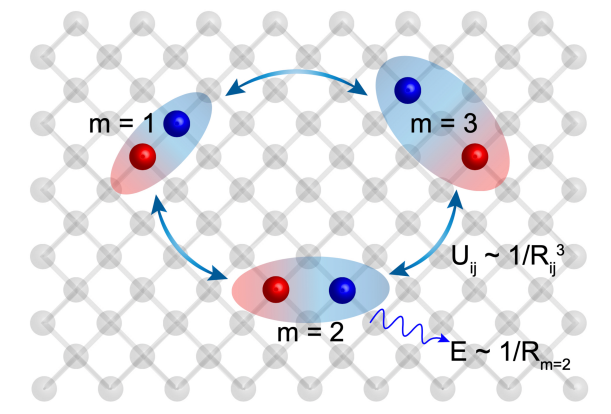


FIG. 2: An illustration of donor-acceptor pairs (DAPs) where the donor and acceptors are first (m=1), second (m=2) and third (m=3) nearest neighbors. The dipole-dipole interaction between DAPs scale as the inverse cube of the distance between the pairs  $(R_{ij})$ . The photon energy emitted from a given shell (m) is proportional to the inverse pair distance  $(R_m)$  between the donor and acceptor of that shell.

dreds of nanoseconds observed for charge recombination in molecular DAP systems [33], paving the way to realizing long-lived states that can be coherently controlled and utilized for quantum applications. The broad variety of DAPs available in different host materials already used for quantum information science highlights the general applicability of the proposed platform.

We present first-principles calculations of the electronic structure of DAPs to understand some of the key properties that are crucial to realize the proposed platform experimentally. We focus our efforts specifically on silicon carbide and diamond, though many other semiconductors may be viable, and the methods presented here are transferable to other systems. First, in order to evaluate whether DAPs could facilitate long-range quantum interactions in the solid-state, we investigate the electronic structure that DAPs form in the bandgap of their host materials. We compute the charge transition levels (CTL) for several donors and acceptors and calculate their binding energies. Then, we determine the zerophonon lines (ZPL) of specific DAPs and predict their photoluminescence (PL) spectra to assess whether individual ZPL from increasingly distant pairs can be experimentally resolved. We compute the magnitude of electric dipole moments that enable DAPs to have optically controllable long-range interactions to show that strong interactions at longer than 10 nm length scales can indeed be realized. Finally, we provide estimates for the radiative lifetimes of some of the DAPs studied here. Our findings indicate that DAPs composed of shallow donors and acceptors exhibit weaker electron-phonon coupling and hence are easier to resolve in photoluminescence spectra. We propose that shallow DAPs may be used as building blocks for realizing an optically addressable, strongly

interacting quantum system in the solid-state.

#### II. RESULTS

Charge Transition Levels -. We analyzed several substitutional defects: boron  $(B_C)$ , nitrogen  $(N_C)$  and phosphorus  $(P_C)$  defects in diamond as well as boron  $(B_C)$ , nitrogen  $(N_C)$  replacing a carbon atom and aluminum  $(Al_{Si})$  replacing a silicon atom in SiC. We first computed the charge transition levels  $(E^f[X^q])$  of all defects (X)as a function of the charge state q, with q=0 and q=1(q = -1) for donors (acceptors) [34]:

$$E^{f}[X^{q}] = E_{tot}[X^{q}] - E_{tot}[bulk] - \sum_{i} n_{i}\mu_{i} + qE_{F} + E_{corr},$$
(1)

where  $E_{tot}[X^q]$  and  $E_{tot}[bulk]$  are the total energies of the supercells containing the defect X and of the pristine bulk, respectively. The integer  $n_i$  indicates the number of atoms of type i (host or defect) that are added or removed from the bulk supercell to create the defect,  $\mu_i$ are the corresponding chemical potentials and  $E_F$  is the Fermi level. The correction term  $E_{corr}$  accounts for the fictitious electrostatic interaction between supercells [35] (see SI for details of the calculations).

Our results are reported in Table I. Calculations using the HSE [36] functional yield results in good agreement with those of previous studies, that are within 0.1 eV of experiment. Note the difference between results obtained with the PBE [37] and HSE functionals in the case of the  $N_C$  donor in diamond, mostly due to the different geometrical distortions predicted by the two functionals. Interestingly the PBE and HSE functionals perform identically for the  $N_C$  shallow donor in 3C-SiC, slightly overestimating its binding energy. The differences between the acceptor levels for  $B_C$  and  $Al_{Si}$  computed at the PBE and HSE level of theory are again due to differences in geometries (see SI).

Electric Dipole Moments - In order to understand whether the DAPs discussed above can be manipulated, we evaluated their electric dipole moments as the difference in polarization  $(\Delta P)$ , on the same branch of the polarization lattice, between the initial (excited) and final (ground) states [50], following Ref. [51, 52]:

$$\Delta P = \frac{1}{\Omega} \left[ \sum_{i} Z_{i} R_{i} - \sum_{n}^{occ} e \bar{\mathbf{r}}_{n} \right], \tag{2}$$

where  $\Omega$  is the volume of the supercell,  $Z_i$  and  $R_i$  are the charges and positions of individual nuclei; e is the electron charge,  $\bar{\mathbf{r}}_n$  is the center of a maximally localized Wannier function (MLWF) [53, 54] and the sum over nruns over all MLWF constructed from the occupied eigenstates of the Kohn-Sham Hamiltonian. Although the electric dipole moments computed using MLWFs [51, 52]

**TABLE I:** Computed charge state transition levels (CTL), referenced in eV to the valence  $(E_V)$  and conduction  $(E_C)$  band edges, for boron  $(B_C)$ , nitrogen  $(N_C)$  and phosphorous  $(P_C)$  in diamond, and boron  $(B_C)$  and nitrogen  $(N_C)$  replacing carbon and aluminum replacing silicon  $(Al_{Si})$  in 3C-SiC. We report results obtained with two density functionals, PBE [37] and HSE [36] as well as results of previous work.

Host	CTL	PBE (HSE)	Previous Work
Diamond <sup>a</sup>	$B_C (0/-)$	$E_V + 0.35 \ (0.35)$	$E_V + [0.37 \text{-} 0.38]^c$
	$N_C (+/0)$	$E_C - 1.47 (1.80)$	$E_C - [1.7-1.9]^d$
	$P_C (+/0)$	$E_C - 1.47 (1.80)$ $E_C - 0.45 (0.47)$	$E_C - [0.5-0.6]^e$
$3C\text{-}SiC^b$	$B_C (0/-)$	$E_V + 0.37 \ (0.57)$	$\begin{bmatrix} E_V + [0.6\text{-}0.73]^{\mathrm{f}} \\ E_C - [0.05\text{-}0.06]^{\mathrm{g}} \end{bmatrix}$
	$N_C (+/0)$	$E_C - 0.16 \ (0.16)$	$E_C - [0.05 - 0.06]^g$
	$Al_{Si} (0/-)$	$E_V + 0.17 (0.19)$	$E_V + [0.24 \text{-} 0.26]^{\text{h}}$

exhibit the same trend as  $eR_m$ , the numerical values differ. As expected, the differences are more pronounced in the case of SiC where a charge transfer between the donor and acceptor occurs. Our results are reported in Figure 4, and we provide in Figure S3 the strength of dipoledipole interactions as a function of distance for two specific cases. The DAPs electric dipole moments can be rather large (> 25 Debye). Comparatively, the nitrogen vacancy center (NV-) has an electric dipole moment of  $\sim 0.8$  Debye [55]. Interestingly, we find that an interaction strength of  $\sim 100$  MHz can be felt from 40 to 90 nm from the DAP, depending on the strength and orientation of the dipoles involved (see SI). Overall, our results point to the feasibility of manipulating DAPs in diamond and SiC. We address next whether the zero-phonon lines (ZPL) of the DAPs may be detectable experimentally and whether ZPLs coming from DAPs located at various distances may be separated from each other.

Zero Phonon Lines – We start by analyzing ZPLs as a function of the distance  $R_m$  and we show that a simple model can accurately reproduce the results obtained with constrained DFT. We then discuss the sensitivity of ZPLs to electric fields. Using constrained DFT [56, 57], the ZPLs were evaluated as the difference between the total energy of the excited state and of the ground state, in their respective optimized geometries, and they were computed as a function of the distance  $R_m$  between the donor and the acceptor. We also computed the value of the ZPLs using a DAP model, where the energy  $\hbar\omega_m$  as a function of  $R_m$  is expressed as [16, 23, 25]:

$$\hbar\omega_m = E_g - (E_A + E_D) + \frac{k_e e^2}{\varepsilon_r r_b} \frac{r_b}{R_m} + J(R_m), \quad (3)$$

where  $E_g$  is the bandgap energy,  $E_D$  and  $E_A$  are the donor and acceptor binding energies calculated from

 $<sup>^{\</sup>rm a}$   $E_g=4.17$  (5.37) eV for the PBE (HSE) functional  $^{\rm b}$   $E_g=1.40$  (2.25) eV for the PBE (HSE) functional

<sup>&</sup>lt;sup>c</sup> Ref. [38, 39], <sup>d</sup> Ref. [39–44], <sup>e</sup> Ref. [45, 46] <sup>f</sup> Ref. [18, 47], <sup>g</sup> Ref. [18, 48, 49], <sup>h</sup> Ref. [47–49]

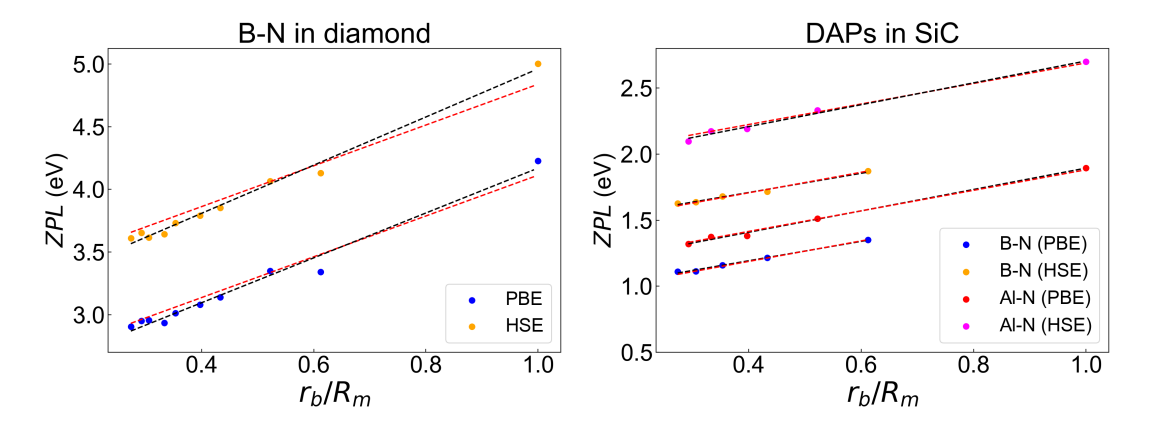


FIG. 3: Calculated zero-phonon line (ZPL) energies using constrained DFT are compared with those obtained with the DAP model of Eq. (3) for both diamond (left) and 3C-SiC (right).  $r_b$  is the equilibrium bond length between nearest neighbor atoms (1.55 Å for diamond, 1.90 Å for SiC) and  $R_m$  is the distance between the donor and acceptor for a given shell (m). Red dashed lines represent Eq. (3) and the black dashed lines are the results obtained from constrained DFT.

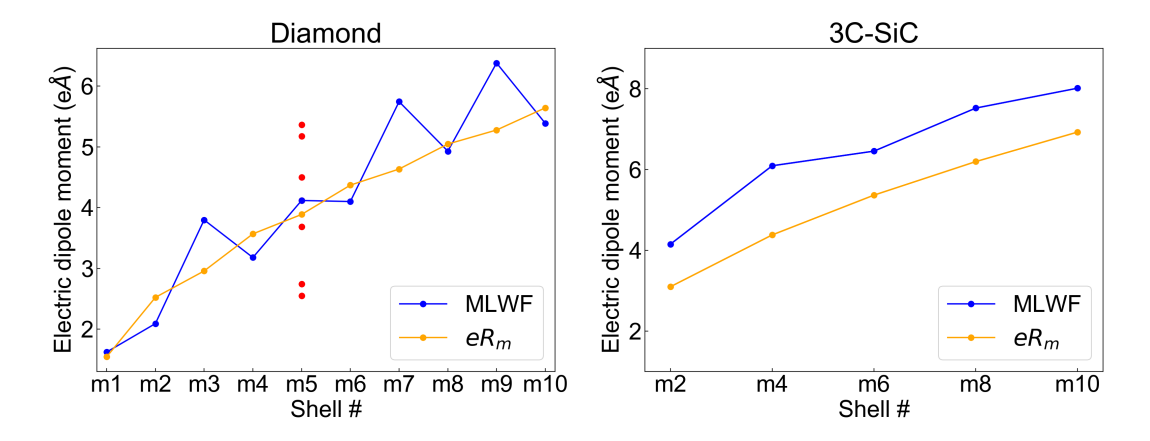


FIG. 4: Electric dipole moments for B-N pairs in diamond (left) and 3C-SiC (right) calculated using maximally localized Wannier functions (MLWF). We calculate the polarization  $\Delta P$  according to Eq. (2), normalize our result with the cell volume  $\Omega$  and report it in dipole moment units. The electric dipole moment is approximately proportional to the distance between the donor and the acceptor  $R_m$  multiplied by the electron charge e. For one case, shell m5, we show how the results (red data points) depend on the relative orientation of the donor and acceptor in the lattice.

Eq. (1) [34], e is the electronic charge,  $\varepsilon_r$  is the long-wavelength dielectric constant, and  $r_b$  is the equilibrium bond length between nearest neighbor atoms of the host material ( $r_b = 1.90 \ (1.55)$  Å for SiC (diamond)). The term  $J(R_m)$  is given by [24, 58]:

$$J(R_m) = \frac{e^2}{4\pi\varepsilon_0\varepsilon_r} \iint_V \psi_D^*(\mathbf{r})\psi_A^*(\mathbf{r}') \left[ \frac{1}{|\mathbf{r} - \mathbf{R_m}|} + \frac{1}{|\mathbf{r}' + \mathbf{R_m}|} - \frac{1}{|\mathbf{r} - \mathbf{R_m} - \mathbf{r}'|} - \frac{1}{|\mathbf{R_m}|} \right] \psi_D(\mathbf{r})\psi_A(\mathbf{r}')d^3\mathbf{r}d^3\mathbf{r}'.$$
(4)

Here,  $\psi_D$  and  $\psi_A$  are the wavefunctions for the electron and hole bound to the donor and the acceptor, respectively (see SI for details).

Our results obtained with constrained DFT and the DAP model are reported in Figure 3 and summarized in the SI (Table S5). The behavior of ZPL as a function of increasing shell number is well reproduced by the DAP model. In particular, the slopes obtained from computed ZPL values for both Al-N and B-N pairs in 3C-SiC are close to the ones predicted by the DAP model. The PBE and HSE functionals yield similar results for B-N and Al-N pairs in 3C-SiC. For B-N DAPs in diamond, the prediction for the slope by the model differs considerably compared to other DAPs in 3C-SiC. This difference stems from the approximation used for the wavefunctions in the DAP model (perturbed Hydrogen-like wavefunctions in the DAP model [24, 58]), which has different ranges of validity depending on the host and pair. In

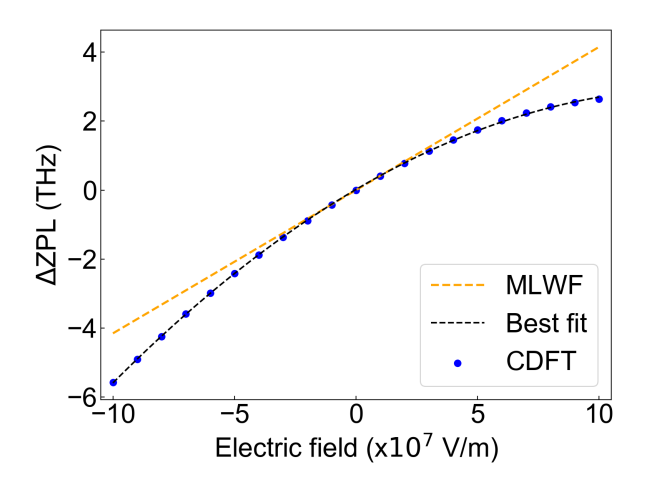


FIG. 5: Computed zero phonon line shift (ΔZPL) for the B-N m5 shell in diamond under homogeneous applied electric field in the (100) direction. The slope at zero field gives the polarization (which can be converted to dipole moment). The dashed orange line indicates the first-order energy shift to ZPL with the slope obtained from maximally localized Wannier functions (MLWF) calculations. The dark blue circles are results obtained from constrained DFT calculations with the PBE functional and the dashed line is a quadratic fit.

particular, such an approximation performs less well for defects that lie deeper in the bandgap, such as the  $N_C$  donor in diamond.

From the y-intercept in Figure 3, we can infer the sum of the binding energies of the donor and acceptor. In all cases, the predicted sums for the binding energies are within 0.1 eV of the calculated combinations of sums of binding energies from Table I. Overall our results show that the DAP model is a useful tool to predict ZPL energies as a function of distance and can provide (semi)-quantitative results.

Next we investigate how individual DAP respond to applied electric fields. As an example, we report in Figure 5 the computed ZPL of the m5 shell in diamond, which shows an extraordinary sensitivity to applied electric fields, with a tunability of the ZPL possible over a few THz. Incidentally, the dipole moment of the DAP can be extracted from the slope at zero field and we find values that compare very well with those obtained above with MLWFs (see SI). The very large dipole moments and broad tunability of DAPs ZPL over many THz, illustrated in Figure 5, show the extreme sensitivity of DAPs to applied electric fields and indicate that DAPs may be suitable candidates for providing long-range interactions in the solid state.

Electron-Phonon Coupling and Photoluminescence Spectra – So far we have demonstrated that DAPs exhibit large electric dipole moments capable of providing optically controllable long-range interactions, and we have shown the sensitivity of ZPLs to electric fields. Next, we investigated whether, in a given host, DAPs at different distances may be optically resolved in experiments. To this end, we compute the photoluminescence (PL) spectra using the effective one-dimensional (1D) configurational coordinate (CC) approximation [60–64]. Within this model, the normalized luminescence lineshape L is given by [65]

$$L(\hbar\omega, T) = \sum_{n,m} w_m(T) |\langle \chi_{em} | \chi_{gn} \rangle|^2$$

$$\times \delta(E_{ZPL} + \hbar\omega_{em} - \hbar\omega_{gn} - \hbar\omega).$$
(5)

The sum is carried over all the vibrational levels with energies  $\hbar\omega_{em}$  and  $\hbar\omega_{gn}$  for excited and ground states;  $w_m(T)$  is the thermal occupation factor and  $\chi$  are the ionic wavefunctions. This formulation of the Franck-Condon approximation assumes that the transition dipole moment is independent of the ionic coordinates [65]. Within this framework each normal mode k contributes to the geometrical distortion of the ions around the defect, with weight  $p_k = (\Delta Q_k/\Delta Q)^2$ , where

$$\Delta Q_k = \sum_{\alpha i} m_{\alpha}^{1/2} \Delta R_{\alpha i} q_{k;\alpha i}; \quad (\Delta Q)^2 = \sum_k \Delta Q_k^2, \quad (6)$$

where  $\alpha$  indexes run over all atoms,  $i = \{x, y, z\}$ ,  $\Delta R_{\alpha i} = R_{e,\alpha i} - R_{g,\alpha i}$  is the vector connecting the ground and excited state geometries;  $q_{k,\alpha i}$  is the unit vector in the direction of the normal mode k. We define effective frequencies associated to the ground and excited states as:

$$\Omega_{\{e,g\}}^2 = \langle \omega_{\{e,g\}}^2 \rangle = \sum_k p_{\{e,g\};k} \omega_{\{e,g\};k}^2$$
(7)

$$S_{\{e,g\}} = \frac{\Omega_{\{e,g\}} \Delta Q^2}{2\hbar},\tag{8}$$

where  $\omega_{\{e,g\};k}$  is the frequency of mode  $q_{\{e,g\};k}$  and  $S_{\{e,g\}}$ are the effective Huang-Rhys (HR) factors for the ground and excited states [66]. The magnitude of the HR factors gives an indication of the strength of the electron-phonon coupling in the system: the smaller the electron-phonon coupling, the easier it should be to distinguish the signal of DAPs located at different distances (i.e. for different shells). We show the calculated parameters from the one-dimensional model in Figure S2 and summarize the results in Table S3. B-N pairs in diamond exhibit a very large HR coupling due to the deep nature of the  $N_C$ donor. The large lattice distortion that  $N_C$  undergoes upon changing its charge state from positive to neutral causes this transition to have a large  $\Delta Q$ , and a large HR coupling. In comparison, B-P pairs have a lower HR coupling, because of the smaller lattice distortions that  $P_C$  experiences upon a charge state transition. As can be seen from Table I and S1,  $Al_{Si}$  is a shallower defect compared to  $B_C$  and it undergoes a smaller geometric

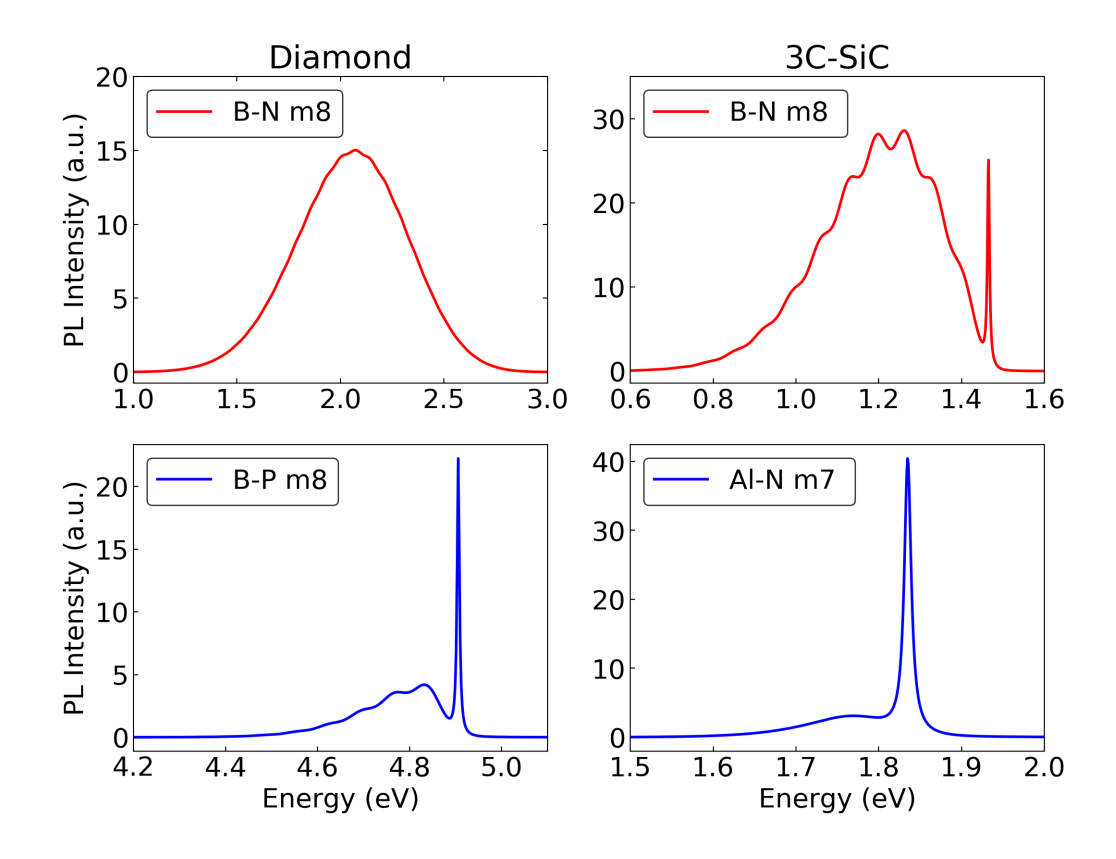


**FIG. 6:** Photoluminescence (PL) spectra obtained from one-dimensional configurational-coordinate diagram using the HSE functional for B-N (m8) and B-P (m8) pairs in diamond, and B-N (m8) and Al-N (m7) pairs in 3C-SiC. PL lineshapes were calculated at 5K using a Lorentzian broadening parameter  $\gamma=3$  meV for the zero-phonon line (ZPL) and a Gaussian broadening parameter  $\sigma=30$  meV for approximating the broadening of the spectral function  $S(\hbar\omega)$  for phonon modes responsible for the phonon side-band (See Ref. [59]).

distortion when changing its charge state; the same is true of the comparison between  $P_C$  and  $N_C$  in diamond.

There are some pronounced differences between the electron-phonon coupling predicted by the PBE and HSE functionals. The total mass-weighted distortions between the ground and excited states ( $\Delta Q$ ) are always larger with the HSE functional. Indeed, PBE predicts most defects to be shallower than HSE and experiment, and this is reflected in the differences between geometric distortions. Hence we conclude that the HSE functional captures the DAP physics more accurately than PBE for two reasons: the position of defect levels within the band gap and the associated lattice distortions upon change of the defect's charge state.

We present in Figure 6 the photoluminescence spectra for the eighth shell (m8) of B-N and B-P pairs in diamond as well as eighth shell (m8) for B-N pairs and the seventh shell (m7) for Al-N pairs in 3C-SiC using the HSE functional. We find that the B-N pairs in diamond exhibit the largest amount of HR coupling ( $\sim$ 20), resulting in a broadband lineshape for the PL spectra, rendering their ZPL not resolvable. In all three other cases, the ZPL

appears to be resolvable. However, B-N pairs in SiC are still a challenging case, as the phonon sidebands from multiple shells overlap and create a broad background. Instead, multiple shells of Al-N pairs in 3C-SiC or B-P pairs in diamond should be distinguishable, given their small phonon sidebands, even if the energy differences between consecutive shells are as small as 5 to 10 meV.

Based on previous work [21, 67], we measured the photoluminescence spectra of eleven diamond samples containing nitrogen and boron, with different grades and preparation. All samples were measured at 4K, with a 407 nm excitation. We selected 2 samples to fabricate electrostatic gates on the surface. Sample details can be found in Table S6 of the SI. From previous observations [21, 67] we anticipated to see many resolvable B-N DAP peaks between 450 nm and 600 nm. We did not observe this in any sample. Moreover, the electrostatic gate measurements revealed that the defects we did observe, did not possess the large electric dipole moments characteristic of DAPs. In this dataset we realized electric fields on the order of a kV/cm through our implanted layer and extracted dipole moments less than 0.5 eÅ. These exper-

iments are consistent with our DFT findings: B-N pairs in diamond have a weak and unresolvable ZPL emission due to their strong phonon coupling.

Instead, our results show that DAPs composed of shallow donors and acceptors should be ideal candidates for resonant and off-resonant manipulation, since there is a smaller electron-phonon coupling and shells that are energetically close together can still be experimentally resolved and isolated from each other. Being able to isolate and manipulate DAPs belonging to larger shell numbers comes with the desired availability of increased electric dipole moments, leading to stronger and consequently longer-range interactions in the solid.

Radiative Lifetimes – Finally, we investigated whether the radiative lifetime of DAPs are sufficiently long to allow for sufficient manipulation of their states. Long lifetimes are generally desirable to allow for various pulse sequences to act on the DAP states. We computed radiative lifetimes for DAPs using the Wigner-Weisskopf theory of fluorescence, and the following expressions [68–70]:

$$\tau = \frac{3\varepsilon_0 h c^3}{2n_r \omega^3 |\mu|^2}; \quad \mu = \frac{e\langle \psi_f | [\hat{H}_{KS}, \mathbf{r}] | \psi_i \rangle}{\epsilon_f - \epsilon_i}$$
 (9)

where  $\mu$  is the optical transition dipole moment, computed following Eq. (9) in Ref. [71], and evaluated in the excited state, where an electron-hole pair is bound to the donor and the acceptor, respectively [70].  $\epsilon_i$  and  $\epsilon_f$  are the eigenvalues of the initial and final states  $\psi_i$  and  $\psi_f$ ,  $\hat{H}_{KS}$  is the Kohn-Sham Hamiltonian,  $\mathbf{r}$  is the position operator,  $n_r$  is the refractive index of the host material and  $\omega$  is the frequency of the optical transition.

In the current literature there is much disagreement about radiative recombination lifetimes of DAPs, depending on the host and defect atoms, ranging from 100s of ps [67] to 100s of  $\mu$ s [16, 17] and even few ms [32]. In addition, temperature and dopant concentration levels play an important role [72] in determining lifetimes. Thomas, Hopfield and Augustyniak [72] observe luminescence in GaP after flash excitation, and their model gives  $\mu$ s range results. However, they also observe less than  $10^{-8}$  second lifetimes for certain closely separated pairs [72]. Ziemelis and Parsons [17] attribute their observation of 70-100  $\mu$ s lifetimes in Si to pairs that are separated by 7.7 to 20 Å. On the other hand, Schneider and Dischler observe 100s of ps of radiative decay times from DAPs in diamond [67].

Our computed radiative recombination lifetimes of DAPs in diamond and 3C-SiC are in the ns range for the first ten shells in diamond; these results are closer to the lifetimes obtained by Schneider and Dischler in their experiments and appear to agree with the observation of less than  $10^{-8}$  second lifetimes for closely-separated pairs [67]. Our predictions for lifetimes in 3C-SiC are longer, in part because of the energy difference involved in the transition between charged states. For example, the B-N transitions in diamond are much more energetic

than B-N or Al-N transitions in SiC, and the approximately one order of magnitude difference in lifetimes is explained through this energy difference. Another order of magnitude difference comes from the optical transition dipole moment. The squared norm of the optical dipole moment is roughly one order of magnitude smaller in 3C-SiC compared to diamond. Together, the differences in energy level positions and optical dipole moment give rise to a two to three order of magnitude difference between the expected lifetimes of B-N pairs in diamond and 3C-SiC. Our results for calculated radiative lifetimes for B-N pairs in 3C-SiC are in the  $\mu$ s range, which are closer to the predictions of Ref [72]. The longer lifetimes found here for pairs in 3C-SiC are an additional reason why these systems would be more desirable for realizing our proposed platform for optically controlled long-range interactions. Radiative lifetimes that are in the  $\mu$ s range can allow for sufficient manipulation of their states with lasers, whereas ns range lifetimes for B-N pairs in diamond would not suffice.

#### III. DISCUSSION

In this work we proposed that DAPs in wide bandgap semiconductors can be engineered as building blocks for coherent long-range interactions in solids. In this platform, the optically switchable dipole moments of DAPs act as the main mediator of the interactions. We presented a detailed analysis of various DAPs in diamond and 3C-SiC using first-principles calculations, aimed at predicting a few crucial properties of these pairs. We showed that DAPs exhibit large, optically switchable dipole moments that are capable of providing the basis for long-range interactions (> 10 nm) in the crystal. We also showed that the ZPL of DAPs show a broad range of tunability. Our estimates for the radiative recombination lifetime in both host materials show that DAPs can have long radiative lifetimes on the order of  $\mu$ s to allow for sufficient manipulation of these states. Additionally, by using a one-dimensional model, we provided an assessment of the amount of electron-phonon coupling specific DAPs would have. We showed that shallower DAPs exhibit smaller electron-phonon coupling due to a modest rearrangement of their geometries when changing their charge state. Shallow DAPs exhibit line spectra that are not overlapping, allowing for experimental resolution of pairs whose ZPL are separated by just a few meV. The combination of several desirable properties of shallow DAPs in SiC pave the way for coherent manipulations of individual DAP shells and optical control of their long-range dipole-dipole coupling in crystals. Our analysis suggests that DAPs are a promising platform to engineer optically addressable long range interactions between point-defects in solids for the realization of quantum technologies.

# IV. METHODS

We determined the electronic structure of donor acceptor pairs in diamond and 3C-SiC using spin-polarised density functional theory (DFT), and the planewave pseudopotential method as implemented in the Quantum Espresso package [73–75]. The calculations of optical transition dipole moments were carried out using the WEST code [76, 77]. We used SG15 ONCV normconserving pseudopotentials [78, 79] and an energy cutoff of 90 Ry. We carried out calculations both with the PBE semi-local functional [37] and the screened hybrid functional by Heyd, Scuseria, and Ernzerhof (HSE) [36]. The screening and mixing parameters for HSE are 0.2  $\rm \AA^{-1}$  and 25% respectively. We used a supercell with 512 atoms for all calculations. The lattice parameters  $(a_0)$ were converged using the PBE (HSE) functional; they are  $a_0 = 3.568(3.543)$  Å for diamond and  $a_0 = 4.381(4.362)$ Å for 3C-SiC, respectively, compared with the experimental values of 3.567 Å for diamond [80] and 4.360 Å for 3C-SiC [81]. All geometries were relaxed with a force threshold of 1 meV/Å. The Brillouin zone of the supercell was sampled at the  $\Gamma$  point only. Further details of geometry optimizations, zero-phonon lines and electronphonon calculations are given in the SI.

# ACKNOWLEDGEMENTS

We thank Professors Ivan G. Ivanov, Tien Son Nguyen and Wolfgang J. Choyke for many fruitful discussions. Additionally, we are grateful to Dr. Bernhard Dischler, Dr. Christoph Wild, Dr. Eckhard Wörner, Dr. Peter Koidl, and Diamond Materials for their insights. We ac-

knowledge Robert Shreiner for his assistance with sample fabrication. This work was supported by AFOSR Grant No. FA9550-22-1-0370. We acknowledge support from Boeing through Chicago Quantum Exchange, and the computational materials science center Midwest Integrated Center for Computational Materials (MICCOM) for the implementation of calculations for transition dipole moments in WEST. We acknowledge funding from NSF QLCI for Hybrid Quantum Architectures and Networks (NSF award 2016136). This work also made use of the shared facilities at the University of Chicago Materials Research Science and Engineering Center, supported by the National Science Foundation under award number DMR-2011854.

## COMPETING INTERESTS

The authors declare no competing interests.

DATA AVAILABILITY

Data that support the findings of this study will be made available through the Qresp [82] curator at https://paperstack.uchicago.edu/explorer.

#### **AUTHOR CONTRIBUTIONS**

A.B. performed all DFT calculations. I.H. and J.E. designed the experimental setup and obtained PL spectra from diamond samples. Y.J. provided useful discussions for calculating PL spectra. H.B., A.H. and G.G designed and supervised the research. A.B. and G.G wrote the manuscript.

- S. S. Gill, A. Kumar, H. Singh, M. Singh, K. Kaur, M. Usman, and R. Buyya, Quantum computing: A taxonomy, systematic review and future directions, Wiley Online Library DOI: 10.1002/spe.3039, 66 (2021).
- [2] S. L. N. Hermans, M. Pompili, H. K. C. Beukers, S. Baier, J. Borregaard, and R. Hanson, Qubit teleportation between non-neighboring nodes in a quantum network, Nature 605, 663 (2022).
- [3] M. Pompili, S. L. N. Hermans, S. Baier, H. K. C. Beukers, P. C. Humphreys, R. N. Schouten, R. F. L. Vermeulen, M. J. Tiggelman, L. dos Santos Martins, B. Dirkse, S. Wehner, and R. Hanson, Realization of a multinode quantum network of remote solid-state qubits, Science 372, 259 (2021).
- [4] C. E. Bradley, J. Randall, M. H. Abobeih, R. C. Berrevoets, M. J. Degen, M. A. Bakker, M. Markham, D. J. Twitchen, and T. H. Taminiau, A ten-qubit solid-state spin register with quantum memory up to one minute, Physical Review X 9, 031045 (2019).
- [5] A. Bourassa, C. P. Anderson, K. C. Miao, M. Onizhuk, H. Ma, A. L. Crook, H. Abe, J. Ul-Hassan, T. Ohshima, N. T. Son, G. Galli, and D. D. Awschalom, Entanglement

- and control of single nuclear spins in isotopically engineered silicon carbide, Nature Materials 19, 1319 (2020).
- [6] N. H. Nickerson, J. F. Fitzsimons, and S. C. Benjamin, Freely scalable quantum technologies using cells of 5-to-50 qubits with very lossy and noisy photonic links, Physical Review X 4, 041041 (2014).
- [7] B. Hensen, H. Bernien, A. E. Dréau, A. Reiserer, N. Kalb, M. S. Blok, J. Ruitenberg, R. F. L. Vermeulen, R. N. Schouten, C. Abellán, W. Amaya, V. Pruneri, M. W. Mitchell, M. Markham, D. J. Twitchen, D. Elkouss, S. Wehner, T. H. Taminiau, and R. Hanson, Loophole-free bell inequality violation using electron spins separated by 1.3 kilometres, Nature 526, 682 (2015).
- [8] D. K. Oh, H. Jeong, J. Kim, Y. Kim, I. Kim, J. G. Ok, and J. Rho, Top-down nanofabrication approaches toward single-digit-nanometer scale structures, Journal of Mechnical Science and Technology 35, 837 (2021).
- [9] P. C. Humphreys, N. Kalb, J. P. J. Morits, R. N. Schouten, R. F. L. Vermeulen, D. J. Twitchen, M. Markham, and R.Hanson, Deterministic delivery of remote entanglement on a quantum network, Nature 558, 268 (2018).

- [10] M. Müller, S. Bounouar, K. D. Jöns, M. Glässl, and P. Michler, On-demand generation of indistinguishable polarization-entangled photon pairs, Nature Photonics 8, 224 (2014).
- [11] C. L. Degen, F. Reinhard, and P. Cappellaro, Quantum sensing, Reviews of Modern Physics 89, 035002 (2017).
- [12] X. Chen, Z. Fu, Q. Gong, and J. Wang, Quantum entanglement on photonic chips: a review, Advanced Photonics 3, 064002 (2021).
- [13] M. Erhard, M. Krenn, and A. Zeilinger, Advances in high-dimensional quantum entanglement, Nature Reviews Physics 2, 365 (2020).
- [14] T. Kazimierczuk, D. Fröhlich, S. Scheel, H. Stolz, and M. Bayer, Giant rydberg excitions in the copper oxide Cu<sub>2</sub>O, Nature 514, 343 (2014).
- [15] A. Browaeys, D. Barredo, and T. Lahaye, Experimental investigations of dipole–dipole interactions between a few rydberg atoms, Journal of Physics B: Atomic Molecular and Optical Physics 49, 152001 (2016).
- [16] W. Schmid, U. Nieper, and J. Weber, Donor-acceptor pair spectra in si:in lpe-layers, Solid State Communications 45, 1007 (1983).
- [17] U. O. Ziemelis and R. R. Parsons, Sharp line donoracceptor pair luminescence in silicon, Canadian Journal of Physics 59, 784 (1981).
- [18] H. Kuwabara, S. Yamada, and S. Tsunekawa, Radiative recombination in  $\beta$ -SiC doped with boron, Journal of Luminescence **12-13**, 531 (1976).
- [19] I. G. Ivanov, A. Henry, F. Yan, W. J. Choyke, and E. Janzen, Ionization energy of the phosporus donor in 3c-SiC from the donor-acceptor pair emission, Journal of Applied Physics 108, 063532 (2010).
- [20] W. J. Choyke and L. Patrick, Luminescence of donoracceptor pairs in cubic SiC, Physical Review B 2, 4959 (1970)
- [21] B. Dischler, W. Rothemund, C. Wild, R. Locher, H. Biebl, and P. Koidl, Resolved donor-acceptor pairrecombination lines in diamond luminescence, Physical Review B 49, 1685 (1994).
- [22] J. A. Freitas Jr., P. B. Klein, and A. T. Collins, Evidence of donor-acceptor pair recombination from a new emission band in semiconducting diamond, Applied Physics Letters 64, 2136 (1994).
- [23] D. G. Thomas, M. Gershenzon, and F. A. Trumbore, Pair spectra and 'edge' emission in gallium phosphide, Physical Review 133, 1A A269 (1964).
- [24] F. Williams, Donor—acceptor pairs in semiconductors, Physica Status Solidi 25, 493 (1968).
- [25] P. J. Dean, Bound excitons and donor-acceptor pairs in natural and synthethic diamond, Physical Review 139, A588 (1965).
- [26] R. Dingle and M. Ilegems, Donor-acceptor pair recombination in GaN, Solid State Communications 9, 175 (1971).
- [27] Q. Tan, J.-M. Lai, X.-L. Liu, D. Guo, Y. Xue, X. Dou, B.-Q. Sun, H.-X. Deng, P.-H. Tan, I. Aharonovich, W. Gao, and J. Zhang, Donor-acceptor pair quantum emitters in hexagonal boron nitride, Nano Letters 22, 1331 (2022).
- [28] L. Kobr, D. M. Gardner, A. L. Smeigh, S. M. Dyar, S. D. Karlen, R. Carmieli, and M. R. Wasielewski, Fast photo-driven electron spin coherence transfer: A quantum gate based on a spin exchange j-jump, Journal of the American Chemical Society 134, 12430 (2012).

- [29] Y. Wu, J. Zhou, J. N. Nelson, R. M. Strong, M. D. Krzyaniak, and M. R. Wasielewski, Covalent radical pairs as spin qubits: Influence of rapid electron motion between two equivalent sites on spin coherence, Journal of the American Chemical Society 140, 13011 (2018).
- [30] H. Bernien, S. Schwartz, A. Keesling, H. Levine, A. Omran, H. Pichler, S. Choi, A. S. Zibrov, M. Endres, M. Greiner, V. Vuletic, and M. D. Lukin, Probing manybody dynamics on a 51-atom quantum simulator, Nature 551, 579 (2017).
- [31] M. Morgado and S. Whitlock, Quantum simulation and computing with rydberg-interacting qubits, AVS Quantum Sci 3, 23501 (2021).
- [32] S. Kamiyama, T. Maeda, Y. Nakamura, A. Henry, I. G. Ivanov, J. P. Bergman, B. Monemar, T. Onuma, and S. F. Chichibu, Extremely high quantum efficiency of donor-acceptor-pair emission in n and b doped 6h-SiC, Journal of Applied Physics 99, 093108 (2006).
- [33] M. D. Krzyaniak, L. Kbor, B. K. Rugg, B. T. Phelan, E. A. Margulies, J. N. Nelson, R. M. Young, and M. R. Wasielewski, Fast photo-driven electron spin coherence transfer: the effect of electron-nuclear hyperfine coupling on coherence dephasing, Journal of Materials Chemistry C 3, 7962 (2015).
- [34] S. B. Zhang and J. E. Northrup, Chemical potential dependence of defect formation energies in GaAs: Application to ga self-diffusion, Physical Review Letters 67, 2339 (1991).
- [35] C. Freysoldt, J. Neugebauer, and C. G. Van de Walle, Fully ab initio finite-size corrections for charged-defect supercell calculations, Physical Review Letters 102, 1 (2009).
- [36] J. Heyd, G. Scuseria, and M. Ernzerhof, Hybrid functionals based on a screened coulomb potential, Journal of Chemical Physics 118, 8207 (2003).
- [37] J. Perdew, K. Burke, and M. Ernzerhof, Generalized gradient approximation made simple, Physical Review Letters 77, 3865 (1996).
- [38] P. Volpe, J. Pernot, and P. Muret, High hole mobility in boron doped diamond for power device applications, Applied Physics Letters 94, 10 (2009).
- [39] K. Czelej, P. Śpiewak, and K. Kurzydłowski, Electronic structure of substitutionally doped diamond: Spinpolarized, hybrid density functional theory analysis, Diamond and Related Materials 75, 146 (2017).
- [40] A. M. Ferrari, S. Salustro, F. S. Gentile, and W. C. Mack-rodt, Substitutional nitrogen atom in diamond. a quantum mechanical investigation of the electronic and spectroscopic properties, Carbon 134, 354 (2018).
- [41] P. Deák, B. Aradi, M. Kaviani, T. Frauenheim, and A. Gali, Formation of nv centers in diamond: A theoretical study based on calculated transitions and migration of nitrogen and vacancy related defects, Physical Review B - Condensed Matter and Materials Physics 89, 1 (2014).
- [42] J. R. Weber, W. F. Koehl, J. B. Varley, A. Janotti, B. B. Buckley, C. G. Van de Walle, and D. D. Awschalom, Quantum computing with defects, Proceedings of the National Academy of Sciences of the United States of America 107, 8513 (2010).
- [43] F. J. Heremans, G. D. Fuchs, and C. F. Wang, Generation and transport of photoexcited electrons in single-crystal diamond, Applied Physics Letters 94, 10 (2009).

- [44] R. G. Farrer, On the substitutional nitrogen donor in diamond, Solid State Communications 7, 685 (1969).
- [45] J. P. Goss, P. R. Briddon, R. Jones, and S. Sque, Donor and acceptor states in diamond, Diamond and Related Materials 13, 684 (2004).
- [46] R. Kalish, The search for donors in diamond, Diamond and Related Materials 10, 1749 (2001).
- [47] M. V. Rao, P. Griffiths, and O. W. Holland, Al and b ion-implantations in 6H and 3C-SiC, Journal of Applied Physics 77, 2479 (2004).
- [48] J. A. Freitas Jr., S. G. Bishop, P. E. R. relaxNordquist Jr., and M. L. Gipe, Donor binding energies determined from temperature dependence of photoluminescence spectra in undoped and aluminum-doped beta SiC films, Journal of Applied Physics 52, 1695 (1988).
- [49] J. A. Freitas Jr., P. B. Klein, and S. G. Bishop, Optical studies of donors and acceptors in cubic SiC, Material Science and Engineering B11, 21 (1992).
- [50] N. A. Spaldin, A beginners guide to the modern theory of polarization, Journal of Solid State Chemistry 195, 2 (2012).
- [51] R. Resta, Macroscopic polarization in crystalline dielectrics: the geometric phase approach, Review of Modern Physics 66, 899 (1994).
- [52] R. King-Smith and D. Vanderbilt, Theory of polarization of crystalline solids, Physical Review B 47, 1651 (1993).
- [53] G. Pizzi, V. Vitale, and R. Arita, Wannier90 as a community code: new features and applications, Journal of Physics: Condensed Matter 32, 165902 (2020).
- [54] N. Marzari, A. A. Mostofi, J. R. Yates, I. Souza, and D. Vanderbilt, Maximally localized wannier functions: Theory and applications, Review of Modern Physics 84, 1419 (2012).
- [55] J. R. Maze, A. Gali, E. Togan, Y. Chu, A. Trifonov, E. Kaxiras, and M. D. Lukin, Properties of nitrogenvacancy centers in diamond: the group theoretic approach, New Journal of Physics 13, 025025 (2011).
- [56] P. Dederichs, S. Blügel, R. Zeller, and H. Akai, Ground states of constrained systems: Application to cerium impurities, Physical Review Letters 53, 2512 (1984).
- [57] B. Kaduk, T. Kowalczyk, and T. Van Voorhis, Constrained density functional theory, Chemical Reviews 112, 321 (2012).
- [58] F. E. Williams, Theory of the energy levels of donoracceptor pairs, Journal of Physical Chemistry Letters 12, 265 (1960).
- [59] A. Alkauskas, B. B. Buckley, D. D. Awschalom, and C. G. Van de Walle, First-principles theory of the luminescence lineshape for the triplet transition in diamond nv centres, New Journal of Physics 16, 073026 (2014).
- [60] P. T. Ruhoff, Recursion relations for multi-dimensional franck-condon overlap integrals, Chemical Physics 186, 355 (1994).
- [61] A. Alkauskas, J. L. Lyons, D. Steiauf, and C. G. Van de Walle, First-principles calculations of luminescence spectrum line shapes for defects in semiconductors: The example of GaN and ZnO, Physical Review Letters 109, 267401 (2012).
- [62] A. Alkauskas, M. D. McCluskey, and C. G. Van de Walle, Tutorial: Defects in semiconductors - combining experiment and theory, Journal of Applied Physics 119, 181101 (2016).
- [63] Y. Jin, M. Govoni, G. Wolfowicz, S. E. Sullivan, F. J. Heremans, D. D. Awschalom, and G. Galli, Photolumi-

- nescence spectra of point defects in semiconductors: Validation of first-principles calculations, Physical Review Materials 5, 084603 (2021).
- [64] A. Gali, Recent advances in the ab initio theory of solidstate defect qubits, Nanophotonics 12, 359 (2023).
- [65] A. M. Stoneham, Theory of Defects in Solids: Electronic Structure of Defects in Insulators and Semimetals (Oxford University Press, 1975).
- [66] K. Huang and A. Rhys, Theory of light absorption and non-radiative transitions in F-centers, Proc. Royal Soc. 204 (1950).
- [67] H. Schneider, B. Dischler, C. Wild, and P. Koidl, Intrinsic radiative lifetimes of donor-acceptor pair excitations in diamond, Physical Review B 51, 677 (1995).
- [68] A. Gali, Ab initio theory of the nitrogen-vacancy center in diamond, Nanophotonics 8, 1907 (2019).
- [69] A. Alkauskas, C. E. Dreyer, J. L. Lyons, and C. G. Van de Walle, Role of excited states in shockley-read-hall recombination in wide-band-gap semiconductors, Physical Review B 93, 1 (2016).
- [70] J. Davidsson, Theoretical polarization of zero phonon lines in point defects, Journal of Physics: Condensed Matter 32, 385502 (2020).
- [71] C. P. Anderson, E. O. Glen, C. Zeledon, A. Bourassa, Y. Jin, Y. Zhu, C. Vorwerk, A. L. Crook, H. Abe, J. Ul-Hassan, T. Ohshima, N. T. Son, G. Galli, and D. D. Awschalom, Five-second coherence of a single spin with single-shot readout in silicon carbide, Science Advances 8 (2022).
- [72] D. G. Thomas, J. J. Jopfield, and W. M. Augustyniak, Kinetics of radiative recombination at randomly distributed donors and acceptors, Physical Review 140, 202 (1965).
- [73] P. Giannozzi, O. Baseggio, and P. Bonfa, Quantum espresso toward the exascale, Journal of Chemical Physics 152, 154105 (2020).
- [74] P. Giannozzi, O. Andreussi, and T. Brumme, Advanced capabilities for materials modelling with quantum espresso, Journal of Physics: Condensed Matter 29, 465901 (2017).
- [75] P. Giannozzi, S. Baroni, and N. Bonini, Quantum espresso: A modular and open-source software project for quantum simulations of materials, Journal of Physics: Condensed Matter 21, 395502 (2009).
- [76] M. Govoni and G. Galli, Large scale GW calculations, Journal of Chemical Theory and Computation 11, 2680 (2015).
- [77] V. W. Yu and M. Govoni, GPU acceleration of largescale full-frequency GW calculations, Journal of Chemical Theory and Computation 18, 4690 (2022).
- [78] M. Schlipf and F. Gygi, Optimization algorithm for the generation of oncv pseudopotentials, Computer Physics Communications 196, 36 (2015).
- [79] D. R. Hamann, Optimized norm-conserving vanderbilt pseudopotentials, Computer Physics Communications 88, 1 (2013).
- [80] S. Shikata, T. Tanno, T. Teraji, H. Kanda, T. Yamada, and J. Kushibiki, Precise measurements of diamond lattice constant using bond method, Japanese Journal of Applied Physics 57, 11 (2018).
- [81] A. Taylor and R. M. Jones, Silicon Carbide A High Temperature Semiconductor, edited by J. R. O'Connor and J. Smiltens (Pergamon Press, 1960).

- [82] M. Govoni, M. Munakami, A. Tanikanti, J. H. Skone, H. B. Runesha, F. Giberti, J. J. de Pablo, and G. Galli, Qresp, a tool for curating, discovering and exploring reproducible scientific papers, Scientific data 6, 190002 (2019).
- [83] H. Kim, A. K. Ramdas, and S. Rodriguez, Spontaneous symmetry breaking of acceptors in 'blue' diamonds, Physical Review Letters 83, 4140 (1999).
- [84] J. Davidsson, V. Ivády, R. Armiento, N. T. Son, A. Gali, and I. A. Abrikosov, First principles predictions of magneto-optical data for semiconductor point defect identification: the case of divacancy defects in 4H–SiC, New Journal of Physics 20, 023035 (2018).

#### V. SUPPLEMENTAL INFORMATION

# A. Distortions to local geometry

While characterizing the CTL of substitutional defects in diamond and 3C-SiC, we analyzed the distortions to local geometries of these defects at different charge states. These calculations show that the most stable ground state geometry for nitrogen is heavily dependant on its charge state. Positively charged nitrogen exhibits  $T_d$  symmetry, where all four neighboring N-C bonds are 1.56 Å in length, compared to the equilibrium C-C bond length of 1.55 Å. For neutral nitrogen however, this changes dramatically. In this case it is stabilized in  $C_{3v}$  symmetry, with one of the N-C bonds being elongated to 2.04 Å, a 33% change compared to the equilibrium C-C bond length observed in other studies previously [41]. The effect of charge is not as pronounced for boron and phosphorus. The only difference between the neutral and negatively charged state for boron comes from the fact that in the former there is a small Jahn-Teller distortion that elongates one of the B-C bonds [39]. The B-C equilibrium bond length is found to be 1.58 Å, while in the neutral case under the small Jahn-Teller distortion the elongated bond is 1.61 Å. This is consistent with previous experimental observations [83]. For phosphorus, there is no noticeable change between different charge states, and all four neighboring bond lengths for any state are 1.70 Å. The reason that the PBE and the HSE functionals give a very similar characterization of the CTL of  $B_C$  and  $P_C$  is that these defects are both relatively shallow defects in diamond. Consequently, their distortions to local geometries are not very pronounced and the PBE and HSE functionals both predict the same local geometry and the same bond lengths with the surrounding neighboring atoms.

The ground state geometry for the  $N_C$  donor in 3C-SiC does not show any sensitivity to the charge state of  $N_C$ . In both charge states, all four of the neighboring bond lengths are 1.92 Å. This is very similar to the  $P_C$  donor in diamond. In both cases, there is virtually no difference between the local geometries of the negatively charged and neutral charge states. However, for  $P_C$  in diamond, the neighboring bonds are elongated by 10% compared to the equilibrium bond length. This number is only 1% for  $N_C$  in 3C-SiC. The perturbation to the host's local geometry is more noticeable for  $P_C$  in diamond, which manifests as a considerably deeper donor in diamond compared to  $N_C$  in 3C-SiC. On the other hand, both  $Al_{Si}$  and  $B_C$  undergo a mild geometric distortion upon changing their charge state. Both defects show  $C_{3v}(T_d)$  symmetry in their neutral (negative) charge state. In its neutral charge state,  $B_C$  has one elongated bond length at 2.04 A and its three remaining neighboring bonds are 1.94 A. While negatively charged, all four bonds remain at 1.92 Å. For  $Al_{Si}$ , the elongated bond at its neutral charge state sits at 2.03 Å and the three neighboring bonds are 1.98 Å. While negatively charged, all four bonds are 1.99

Host	Defect	q	Symmetry	Bond length
Diamond	$B_C$	0 -1	$C_{3v} \\ T_d$	1.02(3), 1.04(1) 1.02(4)
	$N_C$	0 1	$C_{3v} \ T_d$	0.95(3), 1.33(1) 1.01(4)
	$P_C$	0 1	$T_d$ $T_d$	$   \begin{array}{c}     1.10(4) \\     1.10(4)   \end{array} $
3C-SiC	$B_C$	0 -1	$C_{3v} \\ T_d$	$1.02(3), 1.08(1) \\ 1.01(4)$
	$N_C$	0 1	$T_d \ T_d$	$1.01(4) \\ 1.01(4)$
	$Al_{Si}$	0 -1	$C_{3v} \ T_d$	1.04(3), 1.07(1) 1.05(4)

TABLE S1: Symmetries and ground state geometries of substitutional defects in diamond and 3C-SiC are given based on their respective charge states. Bond lengths are given in units of the calculated diamond equilibrium C-C bond length of 1.55 Å for defects in diamond. For defects in 3C-SiC, the respective equilibrium Si-C bond length of 1.90 Å is used. The numbers in brackets indicate the number of bonds of the given length stemming from each central atom.

Å. The slightly more pronounced distortion that  $B_C$  undergoes compared to  $Al_{Si}$  while changing its charge state is also the reason why  $B_C$  is a deeper acceptor compared to  $Al_{Si}$ .

	B-N (c	diamond)	B-N (	3C-SiC)	Al-N (3C-SiC)	
Shell #	PBE	HSE	PBE	HSE	PBE	HSE
m1	3.57	4.35	_	-	1.37	2.22
m2	3.14	3.88	1.21	1.79	-	-
m3	3.08	3.81	-	-	1.34	2.17
m4	2.98	3.70	1.16	1.69	-	-
m5	2.98	3.69	-	-	1.32	2.15
m6	2.91	3.63	1.13	1.66	-	-
m7	2.87	3.57	-	-	1.31	2.12
m8	2.87	3.57	1.12	1.64	-	-
m9	2.85	3.56	-	-	1.31	2.10
m10	2.84	3.55	1.10	1.62	-	-

**TABLE S2:** ZPL energies for all the DAP in diamond and SiC are reported in units of eV. Note that since both B and N replace C atoms in 3C-SiC, no nearest neighbors are possible. B-N pairs can only form even numbered shells. Similarly, Al-N pairs can only have odd numbered shells.

# B. Electric Dipole Moments

We obtain the electric dipole moments of DAP using two different methods. First by using Eq. (2) with

DAP	ZPL (eV)	$\Delta Q \; (\mathrm{amu}^{1/2} \mathrm{\AA})$	$\hbar\Omega_g~(meV)$	$\hbar\Omega_e~(meV)$	$S_g$	$S_e$
	PBE (HSE)	PBE (HSE)	PBE (HSE)	PBE (HSE)	PBE (HSE)	PBE (HSE)
B-N (SiC) m2	1.21(1.60)	0.521 (0.796)	60.35 (61.90)	46.72 (48.74)	1.96 (4.69)	1.52(3.69)
B-N (SiC) m4	1.16(1.51)	0.627(0.854)	60.03 (61.50)	47.64 (51.18)	2.82(5.36)	2.24(4.46)
B-N (SiC) m6	1.13(1.48)	$0.578 \; (0.767)$	63.13 (67.45)	50.49 (55.54)	2.53(4.75)	2.02(3.91)
B-N (SiC) m8	1.12(1.47)	0.597 (0.781)	63.83 (67.83)	51.65 (56.37)	2.72(4.96)	2.20(4.12)
B-N (SiC) m10	1.10(1.45)	$0.601 \ (0.780)$	63.63 (67.67)	51.47 (56.61)	2.75(4.92)	2.23(4.12)
Al-N (SiC) m1	1.37 (1.90)	0.111(0.112)	75.29 (77.54)	74.52 (76.62)	0.11 (0.12)	0.11(0.12)
Al-N (SiC) m3	1.34(1.86)	0.170(0.206)	70.84 (71.31)	66.28 (61.73)	0.25(0.36)	0.23(0.31)
Al-N (SiC) m5	1.32(1.85)	$0.198 \; (0.239)$	65.37 (66.12)	60.73(57.53)	0.31 (0.45)	0.28(0.39)
Al-N (SiC) m7	1.31(1.84)	$0.213 \ (0.274)$	63.91 (66.40)	57.99 (53.80)	0.35 (0.60)	0.31(0.48)
Al-N (SiC) m9	$1.31\ (1.82)$	$0.222 \ (0.314)$	66.10 (67.78)	59.34 (52.07)	0.39 (0.80)	0.35 (0.61)
B-N (diamond) m2	3.14 (3.88)	1.431 (1.498)	69.09 (70.77)	77.72 (84.97)	16.91 (19.00)	19.03 (22.82)
B-N (diamond) m5	2.98(3.69)	1.439(1.501)	68.74 (70.89)	78.80 (85.67)	$17.02\ (19.10)$	19.51 (23.09)
B-N (diamond) m8	2.87(3.57)	$1.428 \ (1.472)$	68.75 (71.31)	80.06 (87.52)	16.77 (18.48)	19.53 (22.68)
B-P (diamond) m2	3.97 (5.10)	0.184 (0.239)	92.60 (86.43)	90.20 (81.33)	0.37(0.59)	0.37(0.56)
B-P (diamond) m5	3.90(5.00)	0.231(0.420)	83.45 (70.08)	78.86 (57.73)	0.53(1.48)	0.50(1.22)
B-P (diamond) m8	3.83 (4.91)	$0.252\ (0.470)$	80.61 (69.49)	76.87 (56.23)	0.61 (1.84)	0.58 (1.49)

**TABLE S3:** Calculated parameters for the effective one-dimensional model for DAP in 3C-SiC and diamond. ZPL energies and total mass-weighted distortion  $\Delta Q$  are given as well as effective frequencies  $(\Omega_{\{e,g\}})$  and HR factors  $(S_{\{e,g\}})$  in ground and excited states.

MLWF. The second method is by applying a homogeneous electric field to the supercell, observing the change in ZPL, and evaluating the instantaneous slope at zero field value, as is demonstrated in Figure 5. Table S4 below shows how closely the results from the two methods agree with each other. In Figure 4, we also report a range of values for the electric dipole moment of the m5 shell in diamond. This is because the specific orientations of the donor and the acceptor in the crystal, not just the pair distance, have an effect on the final dipole moment observed.

Shell # (dir)	Dipole moment (eÅ)		
	Best fit	MLWF	
m5 (100)	-1.71	-1.72	
m5 (010)	1.49	1.65	
m5 (001)	3.13	3.36	
m4 (100)	-3.19	-3.18	
m6 (100)	1.53	1.76	

TABLE S4: Comparison between the MLWF and the best fit methods for a select few B-N pairs in diamond. The dipole moments are reported in units of eÅ. The direction of the applied electric field is given in parenthesis in the first column. Only the component of the dipole moment parallel to the direction of the applied electric field is reported.

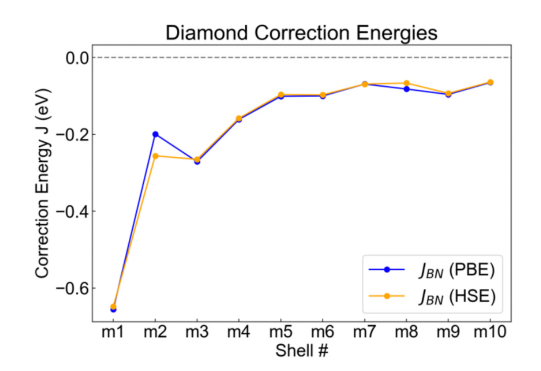
# C. Zero Phonon Lines & J(R<sub>m</sub>) correction

As can be seen in Table S2, the ZPL energies decrease with increasing shell number and inter-defect distance. This is in qualitative agreement with Eq. (3). It is well known that the PBE functional often underestimates the ZPL energy [84]. Therefore, it is not surprising that the results obtained with the HSE functional have slightly more energy than those obtained using PBE. The results obtained for explicitly calculated  $J(R_m)$  correction integrals are presented in Figure (S1). These integrals are calculated using KS orbitals corresponding to the hole and electron wavefunctions bound to acceptors and donors respectively. As expected, this correction term is significant especially for small pair separations [16, 21, 23], and approaches zero as the pair separation is increased. We find that the magnitudes for correction energies in the first few shells are in the expected range according to previous calculations and observations [21, 58]. The ZPL values obtained from constrained DFT already include the effects captured by  $J(R_m)$ . Therefore, in Figure 3, we subtract  $J(R_m)$  from constrained DFT values to compensate for this effect.

We present in Table S5 a summary of results obtained from Figure 3. The theoretical value for the slope  $k_e e^2/\varepsilon_r r_b$  is 1.64 (0.78) eV for diamond (3C-SiC) when  $\varepsilon_r = 5.7$  (9.72) and  $r_b = 1.55$  (1.90) Å are used.

	B-N (diamond)					
	PBE	HSE	PBE	HSE	PBE	HSE
slope	1.79		0.73		0.81	0.83
	2.38		0.90	1.42	1.08	1.88
$E_D + E_A$	1.82	2.33	0.50	0.84	0.32	0.38

**TABLE S5:** A summary of results obtained from Figure 3. The slope and y-intercept values for the linear fit are reported in units of eV for both the PBE and the HSE functionals. The sum of the binding energies is determined by subtracting the y-intercept from the bandgap  $E_q$ 



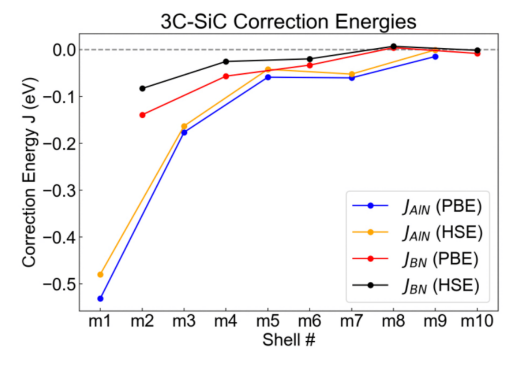


**FIG. S1:**  $J(R_m)$  correction energies are presented as a function of shell number in diamond and 3C-SiC.

# D. Huang-Rhys Factors & Electron-Phonon Coupling

In Table S3 we report the calculated effective ground and excited frequencies  $\Omega_{\{e,g\}}$  and effective HR factors  $S_{\{e,g\}}$ . The mass-weighted distortion  $\Delta Q$  and ZPL belonging to each shell are also included. The effective one-dimensional frequencies extracted from a parabola fit to the ground and excited state potential energy surfaces in the CC diagrams in Figure 6 are reported as well. Figure S2 is a visualization of the data presented in this table.

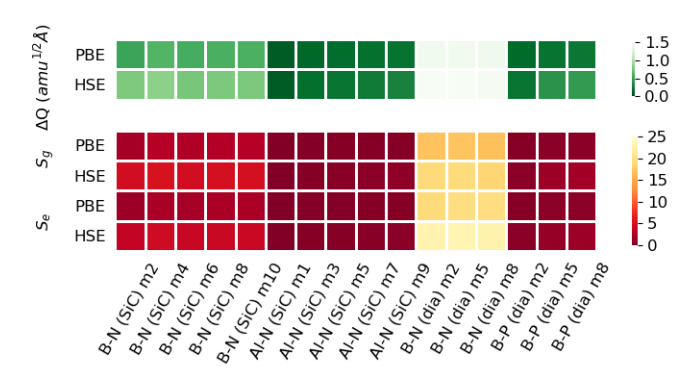


**FIG. S2:** Visualization of calculated parameters from the effective one-dimensional model for DAP in 3C-SiC and diamond. Total mass-weighted distortion  $\Delta Q$  are given as well as HR factors  $(S_{\{e,g\}})$  in ground and excited states.

## E. Analysis of dipole-dipole interaction strengths

The interaction strength between two electric dipoles is given by the formula

$$E_{dd} = \frac{p_i p_j}{4\pi\epsilon_0 \varepsilon_r} \frac{1}{r_{ij}^3} f(\theta_1, \theta_2, \zeta)$$
 (S2)

where  $f(\theta_1, \theta_2, \zeta)$  ranges between -2 and 2 and depends on the relative twist angles the dipoles make with respect to each other and relative to the axis connecting the two dipoles. We plot the interaction strength in MHz with respect to the distance between the two dipoles for several dipole strengths. We take the value  $f(\theta_1, \theta_2, \zeta)$  to be 1 and the dielectric constant as 9.72 for 3C-SiC. In the plot we include the dipole-dipole interaction resulting from two NV- centers interacting in diamond as well, with a different dielectric constant of 5.7. We assume an electric dipole moment of 5 eÅ for small shell numbers and 15 eÅ for relatively large shell numbers. Based on these parameters, it can be seen that an interaction strength of  $\sim 100$  MHz can easily be obtained from 40 to 90 nm away, depending on the strength of the dipoles involved. If even larger dipoles from larger shell numbers can be successfully controlled and manipulated, this interaction strength might be obtained from >100 nm away. Depending on the orientation of DAP with respect to each other, this distance could be slightly different, in either direction.

# F. Experimental Investigations

Samples were placed in a Montana S200 onto a fixed copper post. All samples were addressed with a 0.5 NA Mitutoyo G Plan Apo 50X objective. Photoluminescence

C 1	I m I	C + +: [N/D] / )	T (' (1 1 [NI/TD]	A 1.
Sample	Type	Concentration [N/B] (ppm)	Incorporation method [N/B]	Annealing
1	НРНТ	700/0.1	Innate/Ion Implantation	$800C\ 5\ hours\ Ar/H_2$
2	HPHT	700/1.0	Innate/Ion Implantation	$800C\ 5\ hours\ Ar/H_2$
3	HPHT	700/10	Innate/Ion Implantation	$800C\ 5\ hours\ Ar/H_2$
4	HPHT	700/100	Innate/Ion Implantation	$800C\ 5\ hours\ Ar/H_2$
5	CVD: Optical	0.6/10	Innate/Ion Implantation	$800C\ 5\ hours\ Ar/H_2$
6	CVD: Optical	10/0.05	Ion Implantation/Innate	$800C\ 5\ hours\ Ar/H_2$
7	CVD: Optical	10/10	Ion Implantation	$800C\ 5\ hours\ Ar/H_2$
8	CVD: Optical	0.6/0.5	Innate	
9	CVD: Electronic	1.0/1.0	Ion Implantation	$800C\ 5\ hours\ Ar/H_2$
10	CVD: Electronic	1.0/1.0	Ion Implantation	400C 8 hours, 800C 8 hours, 1200C 2 hours Ar/H <sub>2</sub> Diacid boil
11	CVD: Electronic	10/10	Ion Implantation	400C 8 hours, 800C 8 hours, 1200C 2 hours Ar/H <sub>2</sub> Diacid boil

**TABLE S6:** The details for sample preparation are given below for the eleven diamond samples. Implantation type, concentration and annealing conditions are given for each sample.

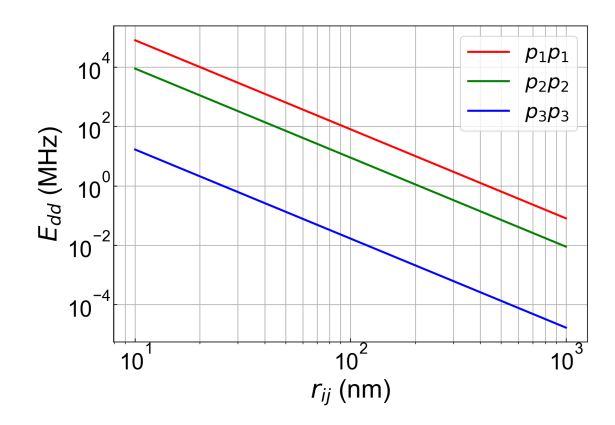


**FIG. S3:** The dipole-dipole interaction strength (MHz) of two dipoles in 3C-SiC. The magnitudes of the two dipoles are assumed to be  $p_2=5$  eÅ (green) for small shell numbers and  $p_1=15$  eÅ (red) for relatively large shell numbers. The dipole-dipole interaction resulting from two NV- centers in diamond,  $p_3=0.166$  eÅ, is also included for comparison (blue).

was generated with a Thorlabs L405P150 operating at 130 mW and directed to the sample with a dichroic mirror (Thorlabs DMPL425L). Spectra was focused directly into the spectrometer with an achromatic lens (Thorlabs AC-508-300-A-ML). Excess laser light was blocked from the spectrometer with two filters: Semrock BLP01-405R-25 and Newport FSR GG420. Our spectrometer is a Princeton Instruments HRS-500, with a PIXIS 400 CCD camera and a 1200g/mm grating blazed at 750nm. The details about sample preparation details are included in Table S6